Kinetic Limit of Heterogeneous Melting in Metals

Dmitriy S. Ivanov* and Leonid V. Zhigilei†

Department of Materials Science and Engineering, University of Virginia, 395 McCormick Road, Charlottesville, Virginia 22904-4745, USA

(Received 7 January 2007; published 9 May 2007)

The velocity and nanoscale shape of the melting front are investigated in a model that combines the molecular dynamics method with a continuum description of the electron heat conduction and electron-phonon coupling. The velocity of the melting front is strongly affected by the local drop of the lattice temperature, defined by the kinetic balance between the transfer of thermal energy to the latent heat of melting, the electron heat conduction from the overheated solid, and the electron-phonon coupling. The maximum velocity of the melting front is found to be below 3% of the room temperature speed of sound in the crystal, suggesting a limited contribution of heterogeneous melting under conditions of fast heating.

DOI: 10.1103/PhysRevLett.98.195701 PACS numbers: 64.70.Dv, 02.70.Ns, 61.80.Az, 68.08.−p

The mechanisms and kinetics of heterogeneous melting have been extensively studied both experimentally and theoretically, resulting in a well-established framework for semiempirical description of the kinetics of the melting process [1–6]. Most of the investigations, however, have been focused on the regime of relatively low overheatings of the liquid-crystal interface above the equilibrium melting temperature, when either the nonequilibrium kinetic description reduces to a linear relationship between the velocity of the melting front and overheating [5,6] or the melting process is considered to be heat flow limited and the overheating is neglected altogether. The analysis of the kinetics of the melting process at strong overheatings is challenging and understanding of the kinetic limits of heterogeneous melting remains poor. In particular, in the absence of more reliable estimates, the speed of sound is often used as the limiting velocity of the melting front in interpretation of the results of short pulse laser melting experiments [4,7–10], where the conditions for significant overheating can be readily achieved. In this Letter, we report the results of molecular dynamics (MD) simulations of heterogeneous melting of a metal sample performed for a range of overheatings extending up to the stability limit of the superheated crystal, when a massive homogeneous nucleation of liquid regions occurs within picoseconds. The velocity and nanoscale stability of the melting front are investigated and the role of the electron heat conduction and electron-phonon coupling in defining the kinetic limit of heterogeneous melting is revealed.

Simulations reported in this Letter are performed for nickel, with interatomic interaction described by the embedded-atom method (EAM) in the form suggested in Ref. [11]. Some of the properties of the EAM Ni material relevant to the melting process are given in Ref. [12]. The systems used in the simulations are fcc crystals of two different sizes, $3.5 \times 3.5 \times 50.1$ nm (56 800 atoms) and $22 \times 22 \times 100$ nm (3 945 600 atoms). The initial systems are equilibrated at zero pressure and temperatures corresponding to given values of overheating. Melting is then initiated by introducing a free (001) surface at one end of the computational cell while keeping two monolayers of the fcc lattice rigid at the opposite side.

Two series of MD simulations are performed in order to elucidate the effect of the electron heat conduction and electron-phonon coupling on the melting process. In the first series, performed with the smaller system, a constant lattice temperature is maintained throughout the computational cell during the simulation. To avoid the local temperature drop at the interface due to the thermal energy transfer to the latent heat of melting, the system is divided into 1 nm layers and the temperature is maintained by the Gaussian thermostat method [13] applied to each individual layer. In the second series of simulations, performed for the larger system, the goal is to investigate the effects of the heat transfer on the velocity of the melting front. In this case the electron heat conduction and electron-phonon coupling are accounted for within the combined atomistic-continuum model [12], where the classical MD method is incorporated into the general framework of the two-temperature model (TTM) [14] describing the time evolution of the lattice and electron temperatures by two coupled nonlinear differential equations. A detailed description of the TTM-MD model and the temperature dependent parameters of the TTM equation for the electron temperature are given in Ref. [12]. One difference from the description presented in [12] is that in the present work we solve the TTM equation for the electron temperature in three dimensions, allowing for the energy redistribution in the directions parallel to the melting front.

The velocities of the melting front in the first series of simulations (constant lattice temperature) are shown by solid diamonds in Fig. 1. At overheatings up to $\sim 1.13 T_m$, the velocity of the melting front propagation increases almost linearly with temperature, whereas a steeper nonlinear increase is observed at higher temperatures. The maximum velocity of the melting front propagation is 600 m/s (12% of the room temperature speed of sound measured for the EAM Ni material, $\nu_s = 5080$ m/s) at

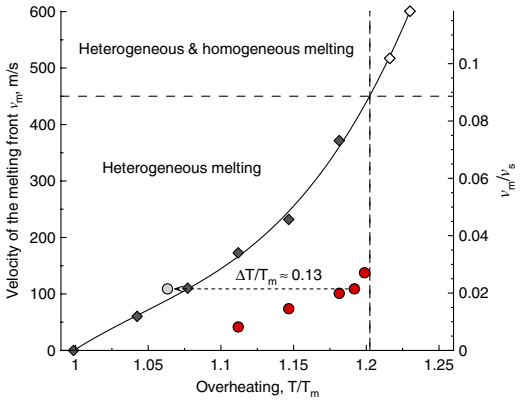

FIG. 1 (color online). The velocity of the melting front propagation in EAM Ni crystal as a function of the overheating. The results of MD simulations performed at constant lattice temperature maintained throughout the system are shown by diamonds. The solid line is a guide to the eye. The vertical dashed line marks the value of overheating above which homogeneous nucleation of liquid regions inside the superheated crystal is observed. The velocities of the melting front in the simulations where both homogeneous and heterogeneous melting is observed are shown by open diamonds. Dark gray (red) circles show the velocities of the melting front in TTM-MD simulations where constant electron temperature is maintained in the bulk of the system and the temperature at the melting front is defined by the transfer of the lattice thermal energy to the latent heat of melting, the electron heat conduction from the bulk, and the electron-phonon coupling (see text for details). The data points shown by dark gray (red) circles are for temperatures of the bulk; if values of local temperatures at the melting front are used (see Fig. 2) the points shift closer to the results obtained in simulations with enforced constant temperature, as shown for a simulation performed at a bulk temperature of $1.19T_m$ by a dashed arrow.

$T = 1.23T_m$. At this and a lower temperature of $1.216T_m$, however, a homogeneous nucleation of liquid region(s) inside the overheated crystal is observed along with the melting front propagation from the free surface. Above $1.23T_m$, we observe homogeneous melting within several picoseconds and the velocity of the melting front cannot be defined.

In the simulations discussed above, the velocity of the melting front is measured for the conditions of a constant temperature enforced throughout the computational cell. In a real melting process, however, the energy supply to the melting region is not instantaneous but is defined by the electron thermal conductivity and electron-phonon coupling. To provide a realistic description of the energy supply to the melting front from the bulk of the overheated crystal we perform a series of TTM-MD simulations in which, instead of enforcing a constant lattice temperature throughout the computational cell, we only maintain a constant electron temperature at the back surface of the computational cell while allowing both electron and lattice temperatures to evolve freely during the melting process. The results of the simulations are shown by dark gray (red) circles in Fig. 1. The velocities of the melting front are

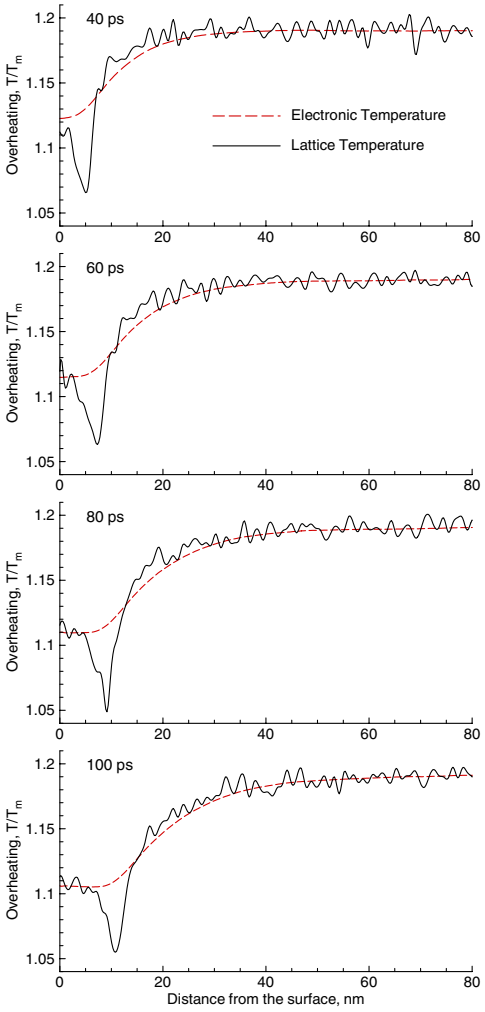

FIG. 2 (color online). Lattice and electron temperature distributions in a TTM-MD simulation of an overheated crystal with a melting front propagating from a free surface. The lattice and electron temperatures are shown by solid and dashed lines, respectively. Constant temperature of $1.19T_m$ is maintained at the depth of 100 nm under the surface.

significantly lower as compared to the ones measured in the constant lattice temperature series. The maximum velocity, measured at $1.2T_m$, is 140 m/s, less than 3% of the room temperature speed of sound in the EAM Ni crystal. Further increase of the temperature results in a homogeneous nucleation of liquid regions inside the overheated crystal, ahead of the melting front.

The decrease in the melting front velocities is related to the transfer of a part of the thermal energy to the latent heat of melting, leading to the local temperature drop in the melting front region. For example, lattice and electron temperature distributions are shown in Fig. 2 for a simulation performed at a temperature of $1.19T_m$. The temperature of $1.19T_m$ is maintained in the bulk of the system, whereas the local lattice temperature at the melting front is significantly smaller and fluctuates around $1.06T_m$. It is the local lattice temperature that defines the velocity of the melting front, and the temperature drop from $1.19T_m$ to

$1.06T_m$ is reflected in the corresponding drop in the melting front velocity from 400 m/s to 109 m/s (from $0.079\nu_s$ to $0.021\nu_s$). Plotting the velocities of the melting front against the local temperature at the melting front shifts the points close and slightly above the line plotted for the simulations with enforced constant lattice temperature, as shown by a dashed arrow in Fig. 1. The depth of the temperature drop at the melting front is defined by the kinetic balance between the energy spent on melting and energy supplied by the electron heat conduction and transferred to the lattice through electron-phonon scattering. The maximum temperature drop would correspond to the conditions of no energy supplied by the heat conduction, $\Delta T^{\max} = \Delta H_m/C_p \approx 0.24T_m$ [12]. A close match of the maximum temperature drop defined by the heat of melting with the limit of overheating for the onset of massive homogeneous melting, $0.23T_m$, agrees with a general trend discussed in Ref. [15]. Because of the energy transfer from the bulk, however, the temperature drop reduces down to $\sim 0.129T_m$ at a bulk temperature of $1.19T_m$ and approaches zero as the bulk temperature approaches T_m. Large differences between the electron and lattice temperatures at the melting front, Fig. 2, are reflecting the finite time needed for electron-phonon equilibration and point to an important role of the strength of the electron-phonon coupling in defining the velocity of the melting front.

The split between the electron and lattice temperatures and the temperature drop at the melting front are larger for metals with weaker electron-phonon coupling. In particular, in simulations performed for Au, a metal with more than an order of magnitude smaller electron-phonon coupling constant (2.1×10^{16} W m^{-3} K^{-1} in Au versus 3.6×10^{17} W m^{-3} K^{-1} in Ni [12]), the temperature drop of $0.15T_m$ is observed in a simulation performed at a bulk temperature of $1.24T_m$, which corresponds to the limit of the crystal stability against the homogeneous melting. The velocity of the melting front at this overheating is 90 m/s, or 3% of the room temperature speed of sound measured for the EAM Au crystal, 3000 m/s.

The relatively low maximum velocity of the melting front, revealed in the simulations, has direct implications for the interpretation of the experimental data on the kinetics of melting. For example, for thin 20 nm Au films used in recent time resolved electron diffraction experiments [7], the melting time shorter than ~70 ps would clearly point to the contribution of the homogeneous nucleation to the melting process [16].

The local temperature drop at the moving melting front not only reduces the maximum velocity of the melting front, but also has a strong effect on the value of the kinetic coefficient, μ, describing the temperature dependence of the velocity of the melting front, ν_m, at small overheatings, in the linear regime, where $\nu_m \approx \mu(T - T_m)$. A kinetic coefficient $\mu = 1.05$ m/(s K) results from the linear fit of the first three data points ($1.04T_m$, $1.08T_m$, $1.11T_m$) obtained in the simulations with reinforced local temperature. In TTM-MD simulations, a much smaller kinetic coefficient of 0.26 m/(s K) can be obtained under the assumption of a linear increase of the interface velocity up to $1.11T_m$. The kinetic coefficient obtained in the TTM-MD

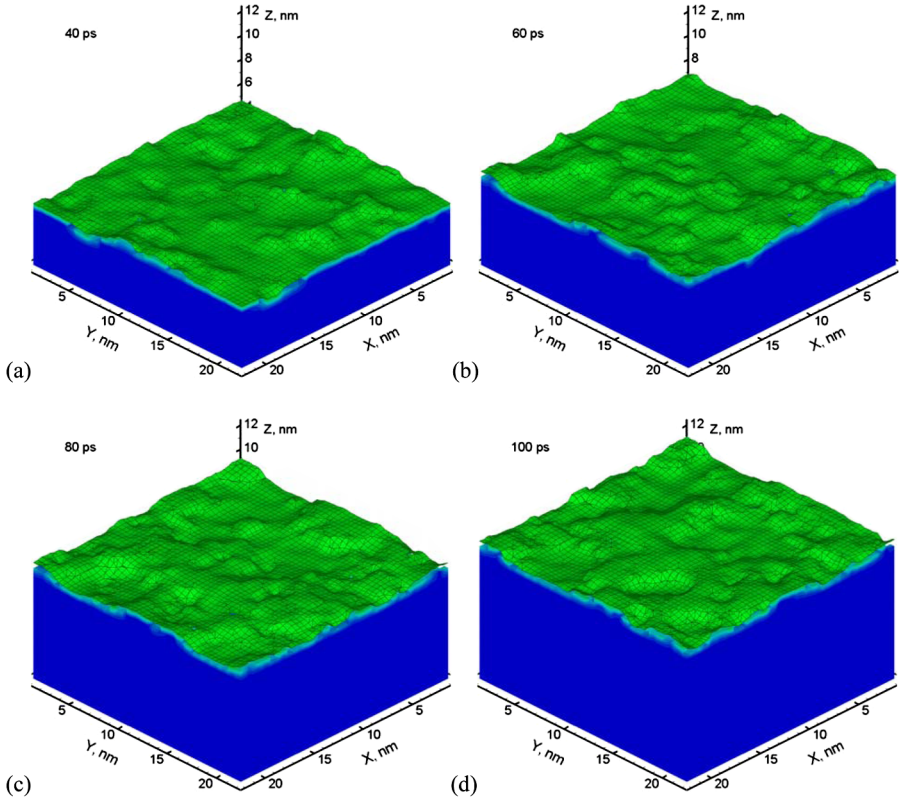

FIG. 3 (color online). Snapshots taken at different times during the TTM-MD simulation illustrated by Fig. 2. The melting starts at the free surface (at the bottom) and the melting front propagates upward, deeper into the bulk of the crystal. The crystalline part of the system is blanked whereas the liquid is shown in dark gray (blue). The solid-liquid interface, shown in light gray (green), is identified using the local order parameter [12] averaged over 1 nm cubic cells. The position of the solid-liquid interface within a partially melted cell is defined based on the amount of liquid phase in the cell.

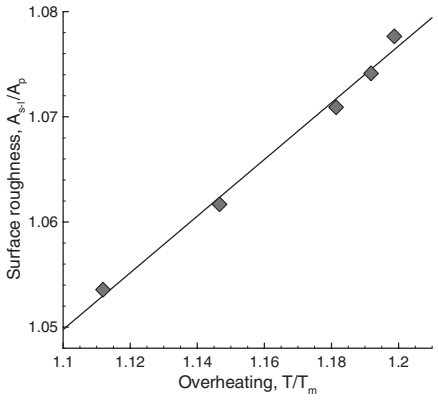

FIG. 4. Deviation of the surface area of the solid-liquid interface, $A_{s\text{-}l}$, from the one of a perfect plane, A_p, shown as a function of the overheating. The line is a linear fit to the data points.

simulations is close to 0.36 m/(s K) measured in earlier MD simulations [5] performed with a different EAM potential for Ni at overheatings up to $1.02T_m$. An average T is maintained in these simulations, the electron heat conduction is not included, and the extent to which the simulation results are affected by the temperature drop at the melting front is not clear. Physically, the velocity of the melting front is a function of the actual lattice temperature at the liquid-crystal interface, and the temperature drop at the melting front should be taken into account in the interpretation of the computational and experimental results.

Propagation of the melting front driven by the energy supply from the bulk of the crystal, Fig. 2, provides the conditions for the appearance of morphological instabilities, when liquid protuberances can emerge and grow into the overheated crystal. While analytical stability analysis can be used to study long-wavelength instabilities [2], MD simulations are capable of investigating the changes in the nanoscale roughness of the melting front as the overheating approaches the limit of crystal stability against homogeneous nucleation.

A visual picture of the evolving solid-liquid interface is shown in Fig. 3 for a TTM-MD simulation performed at $1.19T_m$. The snapshots, taken at equal time intervals during the simulation, show steady state fluctuations of the shape of the melting front. Similar results have been observed in a test simulation performed for a larger system, $44 \times 44 \times 55$ nm (7 948 800 atoms), confirming that the intrinsic size of the surface fluctuations is much smaller than the size of the computational box and the fluctuations are not introduced or affected by the periodic boundary conditions. The characteristic size of the transient features of the interfacial roughness is found to be around 3 nm, with no spatial correlations among the features identified by calculating spatial correlation functions across the melting front. The temperature dependence of the interfacial roughness can be quantified by considering the deviation of the interfacial surface area, $A_{s\text{-}l}$, from that of a perfect plane, A_p. The ratio $A_{s\text{-}l}/A_p$ is plotted as a function of overheating in Fig. 4. While the roughness increases almost linearly with overheating, the temperature dependence is rather weak and the magnitude of the shape fluctuations does not exceed several interatomic distances up to the maximum overheating at which a massive homogeneous nucleation of liquid regions takes place on the time scale of picoseconds.

In summary, the results of TTM-MD simulations of heterogeneous melting at strong overheatings reveal that the temperature dependence of the velocity of the melting front is strongly affected by the local cooling at the moving melting front. In metals, the electron heat conduction from the superheated solid to the melting front and the strength of the electron-phonon coupling are defining the local temperature at the melting front and the velocity of the front propagation. The maximum velocity of the melting front just below the limit of the crystal stability against homogeneous melting is below 3% of the room temperature speed of sound, more than an order of magnitude lower than typically assumed in interpretation of the results of pump-probe laser melting experiments [4,7–9].

Financial support of this work is provided by the National Science Foundation, Grant No. CTS-0348503.

*Present address: National Center for Laser Applications, National University of Ireland, Galway, Ireland.
†Author to whom correspondence should be addressed. Email address: lz2n@virginia.edu

[1] S. R. Coriell and D. Turnbull, Acta Metall. **30**, 2135 (1982).
[2] V. I. Motorin and S. L. Musher, Zh. Tekh. Fiz. **52**, 1200 (1982) [Sov. Phys. Tech. Phys. **27**, 726 (1982)].
[3] J. Q. Broughton, G. H. Gilmer, and K. A. Jackson, Phys. Rev. Lett. **49**, 1496 (1982).
[4] J. Y. Tsao, M. J. Aziz, M. O. Thompson, and P. S. Peercy, Phys. Rev. Lett. **56**, 2712 (1986).
[5] D. Y. Sun, M. Asta, and J. J. Hoyt, Phys. Rev. B **69**, 024108 (2004).
[6] F. Celestini and J.-M. Debierre, Phys. Rev. E **65**, 041605 (2002).
[7] J. R. Dwyer *et al.*, Phil. Trans. R. Soc. A **364**, 741 (2006).
[8] S. I. Ashitkov *et al.*, JETP Lett. **76**, 461 (2002).
[9] A. Rousse *et al.*, Nature (London) **410**, 65 (2001).
[10] B. Rethfeld, K. Sokolowski-Tinten, D. von der Linde, and S. I. Anisimov, Phys. Rev. B **65**, 092103 (2002).
[11] X. W. Zhou *et al.*, Acta Mater. **49**, 4005 (2001).
[12] D. S. Ivanov and L. V. Zhigilei, Phys. Rev. B **68**, 064114 (2003).
[13] D. J. Evans *et al.*, Phys. Rev. A **28**, 1016 (1983).
[14] S. I. Anisimov, B. L. Kapeliovich, and T. L. Perel'man, Zh. Eksp. Teor. Fiz. **66**, 776 (1974) [Sov. Phys. JETP **39**, 375 (1974)].
[15] A. B. Belonoshko, N. V. Skorodumova, A. Rosengren, and B. Johansson, Phys. Rev. B **73**, 012201 (2006).
[16] Z. Lin and L. V. Zhigilei, Phys. Rev. B **73**, 184113 (2006).